Journal Pre-proofs

A control volume scheme using compact integrated radial basis function stencils for solving the Richards equation

Duc Ngo-Cong, Nam Mai-Duy, Diogenes L. Antille, Martinus Th. van Genuchten

Please cite this article as: Ngo-Cong, D., Mai-Duy, N., Antille, D.L., van Genuchten, M.T., A control volume scheme using compact integrated radial basis function stencils for solving the Richards equation, *Journal of Hydrology* (2019), doi: https://doi.org/10.1016/j.jhydrol.2019.124240

A control volume scheme using compact integrated radial basis function stencils for solving the Richards equation

Duc Ngo-Cong[a,*], Nam Mai-Duy[a,b], Diogenes L. Antille[c,d], and Martinus Th. van Genuchten[e,f]

[a]University of Southern Queensland, Institute for Advanced Engineering and Space Sciences, Toowoomba, QLD 4350, Australia.

[b]University of Southern Queensland, School of Mechanical and Electrical Engineering, Faculty of Health, Engineering and Sciences, Toowoomba, QLD 4350, Australia.

[c]CSIRO Agriculture and Food, Canberra, ACT 2601, Australia.

[d]University of Southern Queensland, Centre for Agricultural Engineering, Toowoomba, QLD 4350, Australia.

[e]Federal University of Rio de Janeiro, Department of Nuclear Engineering, Rio de Janeiro, Brazil

[f]São Paulo State University, Center for Environmental Studies, CEA, Rio Claro, Brazil

ABSTRACT

A new control volume approach is developed based on compact integrated radial basis function (CIRBF) stencils for solution of the highly nonlinear Richards equation describing transient water flow in variably saturated soils. Unlike the conventional control volume method, which is regarded as second-order accurate, the proposed approach has high-order accuracy owing to the use of a compact integrated radial basis function approximation that enables improved flux predictions. The method is used to solve the Richards equation for transient flow in 1D homogeneous and heterogeneous soil profiles. Numerical results for different boundary conditions, initial conditions and soil types are shown to be in good agreement with Warrick's semi-analytical

solution and simulations using the HYDRUS-1D software package. Results obtained with the proposed method were far less dependent upon the grid spacing than the HYDRUS-1D finite element solutions.

Keywords: Richards equation; finite volume method; integrated radial basis function; compact stencil; unsaturated flow.

*Corresponding author; Email address: duc.ngo@usq.edu.au (Duc Ngo-Cong)

1. INTRODUCTION

The complex problem of transient water flow in unsaturated or variably-saturated porous media has been widely modelled using the highly nonlinear Richards equation. Neglecting sink/source terms (e.g, root water uptake) and soil and water compressibilities, the Richards equation in its mixed form can be written as (Celia et al., 1990):

$$\frac{\partial \theta(h)}{\partial t} - \nabla \cdot \left[K(h) \nabla h \right] - \frac{\partial K(h)}{\partial z} = 0 \tag{1}$$

where θ and K are, respectively, the volumetric water content and hydraulic conductivity, both being a function of the pressure head h, z is the vertical coordinate (assumed positive upward here), and t is time. It is inherently difficult to obtain numerical solutions of Eq. due to the highly nonlinear nature of the soil hydraulic functions $\theta(h)$ and $K(h)$. Several approaches have been used to deal with nonlinearity of the Richards equation, such as applying Picard iteration (e.g., Celia et al., 1990; Huang et al., 1996) and Newton Raphson (e.g., Lehmann and Ackerer, 1998) methods, the method of lines (e.g., Fahs et al., 2009), or certain transformations (Kirkland et al., 1992; Pan and Wierenga, 1995). The nonlinearities pose especially difficulties under some extreme conditions (e.g., sharp wetting fronts, very dry initial conditions, extreme soil textures, heterogeneous and/or hysteretic soils) using traditional analytical or numerical techniques

(Farthing and Ogden, 2017). For example, finite element solutions often suffer from numerical oscillations near sharp wetting fronts unless very dense grids are used (Celia et al., 1990; Pan and Wierenga, 1995; van Genuchten, 1982).

In the past few years, many numerical schemes have been developed for solving the Richards equation (e.g., Fahs et al., 2009; Farthing et al., 2003; Kavetski et al., 2001; Lehmann and Ackerer, 1998; McBride et al., 2006; Zha et al., 2019). For example, Lehmann and Ackerer (1998) used the modified Picard and Newton iteration schemes to solve both the h-based and mixed forms of the Richards equation governing infiltration in homogeneous and heterogeneous dry porous media. Their results showed that, for the same numerical accuracy, a combination of the modified Picard and Newton scheme required fewer iterations than the modified Picard or Newton schemes as such. Kavetski et al. (2001) introduced an adaptive time stepping with embedded error control to solve the mixed form of the Richards equation. Their second-order adaptive time stepping algorithm improved the performance of the nonlinear solver by providing accurate initial solution estimates for the iterative process. Farthing et al. (2003) formulated a mixed hybrid finite element (MHFE) method and an enhanced cell-centred difference scheme in combination with the method of lines for both the h-based and mixed forms of the Richards equation. Fahs et al. (2009) combined a lumped MHFE method with the method of lines for a more accurate resolution of the Richards equation. They used the lumped MHFE approach (Younes et al., 2006) for approximating the flux to avoid unphysical oscillations for triangular meshes without additional numerical errors. Other recent developments in numerical methods and software for solving the Richards equation can be found in a review paper by Zha et al. (2019).

Warrick et al. (1985) presented a semi-analytical solution to the Richards equation subject to the van Genuchten (1980) soil hydraulic functions. Their solution has been used in many studies as a benchmark for verifying numerical solutions (Caviedes-Voullième et al., 2013; Phoon et al.,

2007). Caviedes-Voullième et al. (2013) presented a finite volume method in combination with four temporal integration schemes to solve the 1D Richards equation. The four schemes included explicit mixed (EM), implicit mixed (IM), explicit pressure head (EP), and implicit pressure head (IP) schemes. They found that the EM and IM schemes produced accurate and conservative solutions, but not the EP and IP schemes. The EM scheme, furthermore, was not able to solve the Richards equation under saturated conditions, while the IM scheme was able to do so. Hayek (2016) further developed an analytical solution of the 1D Richards equation for semi-infinite soils using the special case of an exponential water retention curve and a power law for the hydraulic conductivity. Analytical and semi-analytical solutions of this type are important to test the accuracy of proposed numerical schemes.

In this study we focus on the use of schemes using radial basis functions (RBFs). Such a scheme was first proposed by Kansa (1990) for solving partial differential equations (PDEs) with a high level of accuracy for both gridded and scattered data. Unlike Kansa's approach, Mai-Duy and Tran-Cong (2001) suggested the use of integration to construct the global RBF approximations, which improved the accuracy of numerical solutions. In related work, Wright and Fornberg (2006) presented a generalised finite difference formula based on compact radial basis function approximations for solving partial differential equations on irregular domains with scattered nodes. Šarler and Vertnik (2006) developed a meshless local RBF collocation method for the solution of diffusion problems. The method overcame ill-conditioning problems of the global RBF collocation method (Kansa, 1990) and mitigated the sensitivity problem of choosing the RBF shape parameter. The scheme has been used to solve several industrial problems such as thermo-driven fluid flow problems with a free surface (Hon et al., 2015) and turbulent molten steel flow and solidification (Vertnik et al., 2019). Divo and Kassab (2007) developed an efficient localised meshless

collocation method using the Hardy Multiquadrics RBF for solution of conjugate heat transfer problems.

Schemes using compact integrated radial basis function (CIRBF) stencils were originally proposed by Mai-Duy and Tran-Cong (2011, 2013) for solving partial differential equations. Their CIRBF schemes incorporate not only nodal function values but also nodal values of derivatives into the local integrated radial basis function (IRBF) approximations. Ngo-Cong et al. (2017) presented a generalised finite difference scheme based on the CIRBF approximation to simulate water flow in 1D and 2D heterogeneous soils. Hoang-Trieu et al. (2013) subsequently incorporated the CIRBF approximation into the control volume formulation (called CV-CIRBF) for solving second-order differential problems in one and two dimensions, with application to natural convection flow. Their numerical results show that the CV-CIRBF method yields more accurate results than the standard finite volume method (FVM) and a point collocation CIRBF-based method.

In this article, we further extend the CV-CIRBF method to solve the highly nonlinear Richards equation governing water flow in unsaturated or variably saturated soils. Instead of using the nodal values of the governing equation as in Hoang-Trieu et al. (2013), the nodal second derivatives of a field variable are added into the local IRBF stencils when converting the radial basis function network-weight space into physical space. In the CIRBF scheme of Ngo-Cong et al. (2017), the extra information of second derivatives at some nodal point i were implicitly calculated from the function values at all nodal points over a grid line passing through point i. As a result, this scheme (referred to as a global CIRBF scheme) yielded a fully populated system matrix associated with a grid line. In contrast, the present CV-CIRBF scheme produced a tridiagonal system matrix, which is computationally far more efficient than the global CIRBF scheme. In Section 3.1, we will show that calculations of internodal fluid fluxes using the global CIRBF

scheme (instead of the local CIRBF) can improve the solution accuracy and efficiency in solving the Richards equation. We note that this internodal flux treatment does not affect the tridiagonal system matrix produced by the present CV-CIRBF scheme. A rational function transformation technique (Pan and Wierenga, 1995) in combination with Picard iterations is subsequently employed to treat the nonlinearity of the Richards equation. Our proposed CV-CIRBF method is first illustrated and verified in Section 3.1 through comparisons with the semi-analytical solution of Warrick et al. (1985). The numerical approach is then used in Sections 3.2 and 3.3 to solve several unsaturated flow problems to demonstrate its performance.

2. CONTROL VOLUME – COMPACT INTEGRATED RADIAL BASIS FUNCTION DISCRETISATION OF THE RICHARDS EQUATION

In this section, a control volume approach based on compact integrated radial basis function (CV-CIRBF) stencils is used to discretise the Richards equation governing moisture motion in soils. Consider N_z nodal points on a $z-$grid line. Each node z_i is surrounded by a control volume Ω_i. For interior nodes z_i with $2 \leq i \leq N_z - 1$, Ω_i is defined as $\left[z_{i-1/2}, z_{i+1/2} \right]$. For boundary nodes z_1 and z_{N_z}, the control volumes are $\left[z_1, z_{3/2} \right]$ and $\left[z_{N_z - 1/2}, z_{N_z} \right]$, respectively. In the compact integrated radial basis function (CIRBF) approximation as used by Mai-Duy and Tran-Cong (2011, 2013), the first and second spatial derivatives of the field variable u at a nodal point $z^{(i)}$ are computed as follows:

$$\frac{\partial^2 u^{(i)}}{\partial z^2} = \eta_1 \bar{u} + \eta_2 \left(\frac{\partial^2 u^{(i-1)}}{\partial z^2} \quad \frac{\partial^2 u^{(i+1)}}{\partial z^2} \right)^T \tag{2}$$

$$\frac{\partial u^{(i)}}{\partial z} = \mu_1 \bar{u} + \mu_2 \left(\frac{\partial^2 u^{(i-1)}}{\partial z^2} \quad \frac{\partial^2 u^{(i+1)}}{\partial z^2} \right)^T \tag{3}$$

6

where $\bar{u} = \begin{pmatrix} u^{(i-1)} & u^{(i)} & u^{(i+1)} \end{pmatrix}^T$; η and μ are known vectors of dimension of 1×5;

$\eta_1 = \eta(1:3)$; $\eta_2 = \eta(4:5)$; $\mu_1 = \mu(1:3)$ and $\mu_2 = \mu(4:5)$. Readers are referred to the Appendix

for further detail on the CIRBF approximation. Application of Eqs. and at nodal points

$\hat{z} = \begin{pmatrix} z^{(1)} & z^{(2)} & ... & z^{(N_z)} \end{pmatrix}^T$ on the z-grid line yields

$$\frac{\partial^2 \hat{u}^{(m+1)}}{\partial z^2} = D_{2z}\hat{u}^{(m+1)} + k_{2zk}^{(m)}, \, k_{2zk}^{(m)} = D_{2zk}\frac{\partial^2 \hat{u}^{(m)}}{\partial z^2}, \tag{4}$$

$$\frac{\partial \hat{u}^{(m+1)}}{\partial z} = D_{1z}\hat{u}^{(m+1)} + k_{1zk}^{(m)}, \, k_{1zk}^{(m)} = D_{1zk}\frac{\partial^2 \hat{u}^{(m)}}{\partial z^2}, \tag{5}$$

where $\hat{u} = \begin{pmatrix} u^{(1)} & u^{(2)} & ... & u^{(N_z)} \end{pmatrix}^T$; D_{1z}, D_{1zk}, D_{2z} and D_{2zk} are known matrices of dimension of

$N_z \times N_z$; and (m) and $(m+1)$ are the previous and current time levels for the Picard iteration,

respectively.

Similarly, we apply Eqs. (4) and (5) at $\hat{z}_+ = \begin{pmatrix} z^{(3/2)} & z^{(5/2)} & ... & z^{(N_z-1/2)} & z^{(N_z)} \end{pmatrix}^T$ and

$\hat{z}_- = \begin{pmatrix} z^{(1)} & z^{(3/2)} & ... & z^{(N_z-3/2)} & z^{(N_z-1/2)} \end{pmatrix}^T$ to calculate the second and first derivatives of the

function u at the surfaces of each control volume as follows:

$$\frac{\partial^2 \hat{u}^{(m+1)}}{\partial z^2}\bigg|_+ = D_{2z+}\hat{u}^{(m+1)} + k_{2zk+}^{(m)}, \, k_{2zk+}^{(m)} = D_{2zk+}\frac{\partial^2 \hat{u}^{(m)}}{\partial z^2}, \tag{6}$$

$$\frac{\partial \hat{u}^{(m+1)}}{\partial z}\bigg|_+ = D_{1z+}\hat{u}^{(m+1)} + k_{1zk+}^{(m)}, \, k_{1zk+}^{(m)} = D_{1zk+}\frac{\partial^2 \hat{u}^{(m)}}{\partial z^2}, \tag{7}$$

and

$$\frac{\partial^2 \hat{u}^{(m+1)}}{\partial z^2}_{-} = D_{2z-}\hat{u}^{(m+1)} + k_{2zk-}^{(m)}, \quad k_{2zk-}^{(m)} = D_{2zk-}\frac{\partial^2 \hat{u}^{(m)}}{\partial z^2}, \tag{8}$$

$$\frac{\partial \hat{u}^{(m+1)}}{\partial z}_{-} = D_{1z-}\hat{u}^{(m+1)} + k_{1zk-}^{(m)}, \quad k_{1zk-}^{(m)} = D_{1zk-}\frac{\partial^2 \hat{u}^{(m)}}{\partial z^2}. \tag{9}$$

Here, we adopt the rational function transformation method proposed by Pan and Wierenga (1995) to transfer the pressure head h in Eq. into a transformed function f as follows:

$$f = \begin{cases} \dfrac{h}{1+\beta h} & if\ h < 0 \\ h & if\ h \geq 0 \end{cases} \tag{10}$$

where β is a transformation constant. Rearranging Eq. gives

$$h = \begin{cases} \dfrac{f}{1-\beta f} & if\ h < 0 \\ f & if\ h \geq 0. \end{cases} \tag{11}$$

Taking the derivative of both sides of Eq. and using Eq. (10) to eliminate f results in

$$\frac{\partial h}{\partial f} = \begin{cases} (1+\beta h)^2 & if\ h < 0 \\ 1 & if\ h \geq 0. \end{cases} \tag{12}$$

Making use of the chain rule of partial derivatives, we obtain

$$\nabla \cdot [K(h)\nabla h] = \nabla \cdot \left(K^*(h)\nabla f\right) \tag{13}$$

where $K^* = K\partial h / \partial f$. Substituting Eq. into Eq. gives

8

$$\frac{\partial \theta}{\partial t} - \nabla \cdot \left(K^* \nabla f \right) - \frac{\partial K}{\partial z} = 0. \tag{14}$$

The vertical flux is defined as $q_z = -K^* \partial f / \partial z - K$. The nonlinear term in Eq. is now linearised using the Picard iteration method, which for a one-dimensional system leads to

$$\frac{\theta^{(n+1,m+1)} - \theta^{(n)}}{\Delta t} - \frac{\partial}{\partial z} \left(K^{*(n+1,m)} \frac{\partial}{\partial z} f^{(n+1,m+1)} \right) - \frac{\partial K^{(n+1,m)}}{\partial z} = 0 \tag{15}$$

where the superscript n refers to a physical time level, and m to the Picard iteration. The specific moisture capacity function $C(h) = d\theta / dh$ is transformed as follows:

$$C^* = C \frac{\partial h}{\partial f} = \frac{d\theta}{df}. \tag{16}$$

Application of a Taylor series expansion about the point $f^{(n+1,m)}$ results in

$$\theta^{(n+1,m+1)} = \theta^{(n+1,m)} + C^{*(n+1,m)} \delta + O(\delta^2) \tag{17}$$

where $\delta = f^{(n+1,m+1)} - f^{(n+1,m)}$. Substitution of Eq. into yields

$$\frac{C^{*(n+1,m)}}{\Delta t} \delta - \frac{\partial}{\partial z} \left(K^{*(n+1,m)} \frac{\partial \delta}{\partial z} \right) = \frac{\partial}{\partial z} \left(K^{*(n+1,m)} \frac{\partial f^{(n+1,m)}}{\partial z} \right) + \frac{\partial K}{\partial z} + \frac{\theta^{(n)} - \theta^{(n+1,m)}}{\Delta t}, \tag{18}$$

which can be rewritten in the form:

$$\frac{C^{*(n+1,m)}}{\Delta t} \delta - \frac{\partial}{\partial z} \left(K^{*(n+1,m)} \frac{\partial \delta}{\partial z} \right) = -\frac{\partial q_z^{(n+1,m)}}{\partial z} + \frac{\theta^{(n)} - \theta^{(n+1,m)}}{\Delta t} \tag{19}$$

The Richards equation is now integrated over each control volume Ω_i as follows:

9

$$\int_{\Omega_i} \frac{C^{*(n+1,m)}}{\Delta t} \delta^{(n+1,m+1)} dz - \left(K^{*(n+1,m)} \frac{\partial \delta^{(n+1,m+1)}}{\partial z} \right)(z_{i+1/2}) + \left(K^{*(n+1,m)} \frac{\partial \delta^{(n+1,m+1)}}{\partial z} \right)(z_{i-1/2})$$

$$= -q_z^{(n+1,m)}\left(z_{i+1/2}\right) + q_z^{(n+1,m)}\left(z_{i-1/2}\right) + \int_{\Omega_i} \frac{\theta^{(n)} - \theta^{(n+1,m)}}{\Delta t} dz \tag{20}$$

where the vertical fluxes at the control surfaces $z_{i+1/2}$ and $z_{i-1/2}$ are given by

$$q_z^{(n+1,m)}\left(z_{i+1/2}\right) = -K^{*(n+1,m)}\left(z_{i+1/2}\right)\frac{\partial f^{(n+1,m)}\left(z_{i+1/2}\right)}{\partial z} - K\left(z_{i+1/2}\right) \tag{21}$$

$$q_z^{(n+1,m)}\left(z_{i-1/2}\right) = -K^{*(n+1,m)}\left(z_{i-1/2}\right)\frac{\partial f^{(n+1,m)}\left(z_{i-1/2}\right)}{\partial z} - K\left(z_{i-1/2}\right), \tag{22}$$

respectively, in which the internodal conductivity given by the arithmetic mean of the nodal values, i.e., $K^{*}(z_{i+1/2}) = [K^{*}(z_i) + K^{*}(z_{i+1})]/2$, is assumed constant over each control volume. The integrals in Eq. are approximated using the midpoint rule. Application of Eq. to all control volumes Ω_i on the z-axis results in

$$\left[\frac{\hat{C}^{*(n+1,m)}}{\Delta t} \Delta z.I - \hat{K}_+^{*(n+1,m)} D_{1z+} + \hat{K}_-^{*(n+1,m)} D_{1z-} \right].\hat{\delta}^{(n+1,m+1)} = \hat{K}_+^{*(n+1,m)} k_{1z\delta+} - \hat{K}_-^{*(n+1,m)} k_{1z\delta-}$$

$$-q_z^{(n+1,m)}\left(z_{i+1/2}\right) + q_z^{(n+1,m)}\left(z_{i-1/2}\right) + \frac{\hat{\theta}^{(n)} - \hat{\theta}^{(n+1,m)}}{\Delta t} \Delta z \tag{23}$$

where I is the identity matrix. The first and second spatial derivatives of δ and f at the control surfaces $z_{i+1/2}$ and $z_{i-1/2}$ are discretised by using the CIRBF scheme (Eqs. (6)-(9)) as follows:

$$\frac{\partial^2 \hat{\delta}^{(m+1)}}{\partial z^2}\bigg|_+ = D_{2z+}\hat{\delta}^{(m+1)} + k_{2zk\delta+}^{(m)}, \, k_{2zk\delta+}^{(m)} = D_{2zk+}\frac{\partial^2 \hat{\delta}^{(m)}}{\partial z^2} \tag{24}$$

$$\frac{\partial \hat{\delta}^{(m+1)}}{\partial z}\Bigg|_{+} = D_{1z+}\hat{\delta}^{(m+1)} + k_{1zk\delta+}^{(m)}, \, k_{1zk\delta+}^{(m)} = D_{1zk+}\frac{\partial^2 \hat{\delta}^{(m)}}{\partial z^2} \tag{25}$$

$$\frac{\partial^2 \hat{\delta}^{(m+1)}}{\partial z^2}\Bigg|_{-} = D_{2z-}\hat{\delta}^{(m+1)} + k_{2zk\delta-}^{(m)}, \, k_{2zk\delta-}^{(m)} = D_{2zk-}\frac{\partial^2 \hat{\delta}^{(m)}}{\partial z^2} \tag{26}$$

$$\frac{\partial \hat{\delta}^{(m+1)}}{\partial z}\Bigg|_{-} = D_{1z-}\hat{\delta}^{(m+1)} + k_{1zk\delta-}^{(m)}, \, k_{1zk\delta-}^{(m)} = D_{1zk-}\frac{\partial^2 \hat{\delta}^{(m)}}{\partial z^2} \tag{27}$$

and

$$\frac{\partial^2 \hat{f}^{(m+1)}}{\partial z^2}\Bigg|_{+} = D_{2z+}\hat{f}^{(m+1)} + k_{2zkf+}^{(m)}, \, k_{2zkf+}^{(m)} = D_{2zk+}\frac{\partial^2 \hat{f}^{(m)}}{\partial z^2} \tag{28}$$

$$\frac{\partial \hat{f}^{(m+1)}}{\partial z}\Bigg|_{+} = D_{1z+}\hat{f}^{(m+1)} + k_{1zkf+}^{(m)}, \, k_{1zkf+}^{(m)} = D_{1zk+}\frac{\partial^2 \hat{f}^{(m)}}{\partial z^2} \tag{29}$$

$$\frac{\partial^2 \hat{f}^{(m+1)}}{\partial z^2}\Bigg|_{-} = D_{2z-}\hat{f}^{(m+1)} + k_{2zkf-}^{(m)}, \, k_{2zkf-}^{(m)} = D_{2zk-}\frac{\partial^2 \hat{f}^{(m)}}{\partial z^2} \tag{30}$$

$$\frac{\partial \hat{f}^{(m+1)}}{\partial z}\Bigg|_{-} = D_{1z-}\hat{f}^{(m+1)} + k_{1zkf-}^{(m)}, \, k_{1zkf-}^{(m)} = D_{1zk-}\frac{\partial^2 \hat{f}^{(m)}}{\partial z^2}. \tag{31}$$

Substitution of these equations into Eq. leads to a system of linear equations, which is solved to obtain $\hat{\delta}$ at each physical time step. Note that the resulting system matrix (for the 1D case) has only 3 non-zero entries on each row. At each physical time step, the Picard iteration is terminated when the following criterion is fulfilled

11

$$\sqrt{\frac{\sum\limits_{i=1}^{N_z}\left(f_i^{(m+1)}-f_i^{(m)}\right)^2}{\sum\limits_{i=1}^{N_z}\left(f_i^{(m+1)}\right)^2}}<TOL \tag{32}$$

where *TOL* is a prescribed tolerance, presently set at 10^{-5}.

3. NUMERICAL RESULTS AND DISCUSSION

In this section, the CV-CIRBF method in combination with Picard iteration and the rational function transformation is used to solve the Richards equation in one dimension (1D) for different boundary conditions (constant pressure head and constant flux), initial pressure heads (i.e., $h_0 = -800, -10000$ and -50000 cm) and soil types (relatively coarse-, medium- and fine-textured media). We used the standard van Genuchten-Mualem (VG) model to describe the soil water retention curve, *θ(h)*, and the relative hydraulic conductivity function, *K(h)*, as follows (van Genuchten, 1980):

$$\theta(h)=\begin{cases}\dfrac{\theta_s-\theta_r}{\left[1+\left(\alpha|h|\right)^\eta\right]^\mu}+\theta_r & if\ h\le 0 \\[2mm] \theta_s & if\ h>0\end{cases} \tag{33}$$

$$K(h)=\begin{cases}K_s S_e^{\hat{L}}\left[1-\left(1-S_e^{\frac{1}{\mu}}\right)^\mu\right]^2 & if\ h\le 0 \\[2mm] K_s & if\ h>0\end{cases} \tag{34}$$

where θ_s and θ_r are, respectively, the saturated and residual water contents, α and η are fitting parameters, K_s is the saturated hydraulic conductivity, $S_e = (\theta - \theta_r)/(\theta_s - \theta_r)$ is effective saturation, $\mu = 1 - 1/\eta$, and $\hat{L} = 0.5$. Table 1 presents the van Genuchten-Mualem (VG) hydraulic parameters of the three soils we considered. For the relatively coarse-textured soil we used the hydraulic parameters of a loamy sand as provided by Carsel and Parrish (1988). For the medium soil we took the hydraulic parameters from a study by Vogel and Hopmans (1992) on furrow irrigation. The soil in their study was categorized as a sand but in reality had hydraulic parameters more typical of a medium-textured soil as indicated by the class-pedotransfer functions of Carsel and Parrish (1988) and Schaap et al. (2001). And for the fine-textured soil we used the hydraulic parameters of a clay loam soil as categorized by Carsel and Parrish (1988).

Table 1. Van Genuchten-Mualem (VG) soil hydraulic parameters
of the three soils considered in this study.

Soil texture	van Genuchten hydraulic parameters				
	θ_r (cm³/cm³)	θ_s (cm³/cm³)	α (cm⁻¹)	η (-)	K_s (cm/min)
Coarse	0.057	0.410	0.1240	2.28	0.2431
Medium	0.061	0.420	0.0189	2.00	0.0270
Fine	0.095	0.410	0.0190	1.31	0.0043

θ_r: residual water content; θ_s: saturated water content; α: VG multiplier of the
pressure head; η: VG exponent, K_s saturated hydraulic conductivity.

For all simulations we considered vertical downward infiltration into a 100-cm deep soil profile with the lower boundary at z=0 cm and the upper boundary at z=100 cm. In this study we limited ourselves to fixed nodal spacings (Δz).

3.1 Example 1: Constant pressure head at upper and lower boundaries

Initial and boundary conditions for this first example are $h(z, t = 0) = h_0 = -800$ cm, $h(0, t) = h_{bottom} = -800$ cm, and $h(100, t) = h_{top} = 0$ cm. In this example, we used fixed time steps

(Δt). Internodal fluxes are known to have errors when changes in the water content are significant, especially for heterogeneous soils due to discontinuities in the water content at the interface of different soil layers. In this example, we used two different approaches to calculate the internodal fluxes as given by Eqs. (21) and (22):

- Approach 1: Internodal fluxes are calculated using the present local CIRBF scheme, Eq. (5).

- Approach 2: Internodal fluxes are calculated using the global CIRBF scheme (Ngo-Cong et al., 2017), Eq. .

The CV-CIRBF formulation was verified by comparing results with the semi-analytical solution (Celia et al., 1990). Performance was assessed based on relative error norms between the numerical solutions and the semi-analytical solution of Warrick et al. (1985) at three marks (Fig. 1) corresponding to S_e^*=0.25, 0.5 and 0.75 where $S_e^* = (S_e - S_{e0})/(1 - S_{e0})$ and S_{e0} is the initial effective saturation. Table 2 shows comparisons of the relative error norm, $Ne(z)$, the total number of iterations, and the total CPU time required to obtain the converged solution with TOL=10^{-5}. The relative error norm, $Ne(z)$, is calculated as

$$Ne(z) = \sqrt{\sum_{k=1}^{3}(z_k - \overline{z}_k)^2 / \sum_{k=1}^{3}\overline{z}_k^2} \tag{35}$$

where z_k and $\overline{z}_k$ are the numerical and semi-analytical values at the k-th mark, respectively. The time step was set at 0.5 minutes for all cases. For the purpose of CPU time comparisons, all related computations were carried out on a single 3.10 GHz processor machine with 8 GB RAM.

The CV-CIRBF methods yielded more accurate solutions than the FDM of Celia et al. (1990), with Approach 2 solutions being slightly more accurate than those of Approach 1.

14

Approach 2 was also more efficient than Approach 1 in terms of the total number of iterations and the total CPU time. Since Approach 2 outperformed Approach 1 in terms of accuracy and efficiency, we will use here further only the CV-CIRBF method with Approach 2. For a given grid size, Approach 2 was slower than the FDM. However, Approach 2 achieved a given level of accuracy with a much coarser grid and hence was more efficient. For instance, Approach 2 with a grid of 21 nodes produced better results in 4.16 s than the FDM with a grid of 61 nodes in 5.1 s. Figure 1a shows the influence of the time step on the CV-CIRBF results for the medium-textured soil using $\Delta t = \{0.5, 1, 10, 30\}$ min and a grid of 51 nodes. The Warrick semi-analytical solution (Phoon et al., 2007; Warrick et al., 1985) and the finite difference method (FDM) results of Celia et al. (1990) are also depicted for comparison purposes. Distributions of the pressure head for different grid sizes $N_z = \{21, 51\}$ and $\Delta t = 0.5$ min are described in Fig. 1b. The results indicate that the present method yields more accurate solutions when refining the grid and time step sizes and that the CV-CIRBF solutions are more accurate than those based on the FDM scheme.

Table 2. Example 1: Comparisons of the relative error norm (*Ne*), total number of iterations, and total CPU time required to obtain converged solutions with TOL=10^-5 between the FDM and CV-CIRBF using Approaches 1 and 2. The time step was set at 0.5 minutes for all cases. FDM, App.1 and App. 2 stand for the finite difference method of Celia et al. (1990), Approach 1 and Approach 2, respectively.

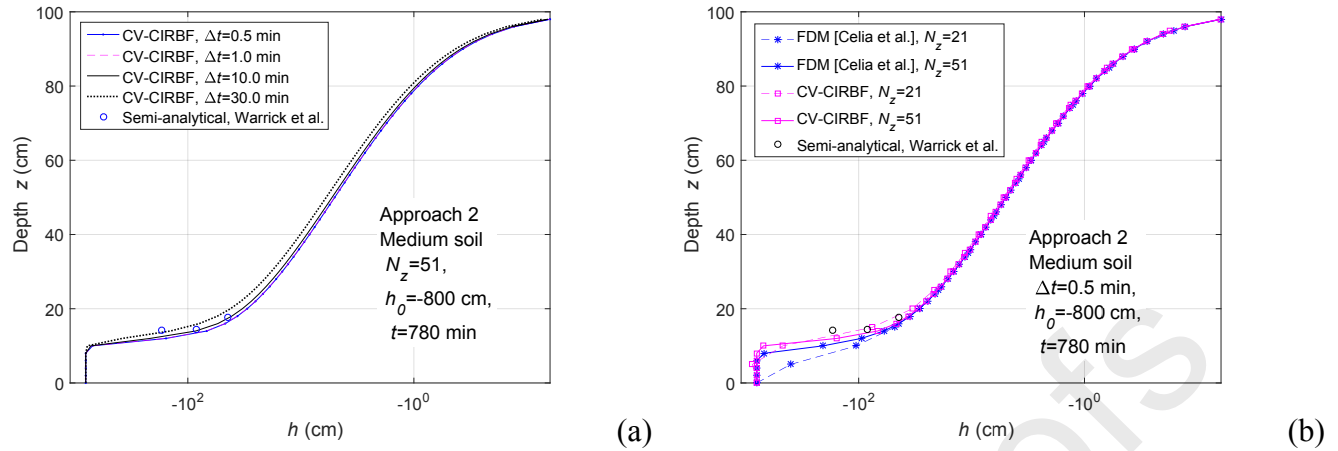|	*Ne(z)*			Number of iterations			CPU time (seconds)		
Grid	FDM	App. 1	App. 2	FDM	App. 1	App. 2	FDM	App. 1	App. 2
21	2.25E-01	4.63E-02	4.20E-02	4735	7947	4737	3.86	6.27	4.16
31	1.91E-01	5.91E-02	5.91E-02	4788	7451	4789	4.03	6.66	4.37
41	1.80E-01	7.77E-02	7.77E-02	4847	7537	4846	4.28	7.21	4.69
51	1.58E-01	9.53E-02	9.53E-02	4937	7591	4898	4.73	7.95	5.22
61	1.44E-01	9.82E-02	9.81E-02	5104	7638	4929	5.10	8.34	5.42

15

Figure 1. Calculated pressure head (h) distributions versus depth (z) obtained with the CV-CIRBF method using different time steps Δt (a) and nodal spacings (b), compared with the semi-analytical solution of Warrick et al. (1985) (a, b) and the finite difference solution (FDM) of Celia et al. (1990) (b). Calculations are for the medium-textured soil subject to ponded infiltration.

Figure 2 compares similar pressure head distributions versus depth, now at four different times, with results obtained using both the semi-analytical solution of Warrick et al. (1985) and the HYDRUS-1D software of Šimůnek et al. (2008). Results show a slightly better performance of the CV-CIRBF scheme as compared to HYDRUS-1D. Calculations in Fig. 2 were obtained for an initial condition of -800 cm. Results for more extreme initial conditions of -10,000 cm and -50,000 cm are shown in Fig. 3 assuming nodal spacings of 5 and 2 cm (i.e., N_z values of 21 and 51, respectively). The distributions indicate only a marginal effect of nodal spacing on the CV-CIRBF results, but with the HYDRUS-1D distributions depending far more on the number of finite element nodes.
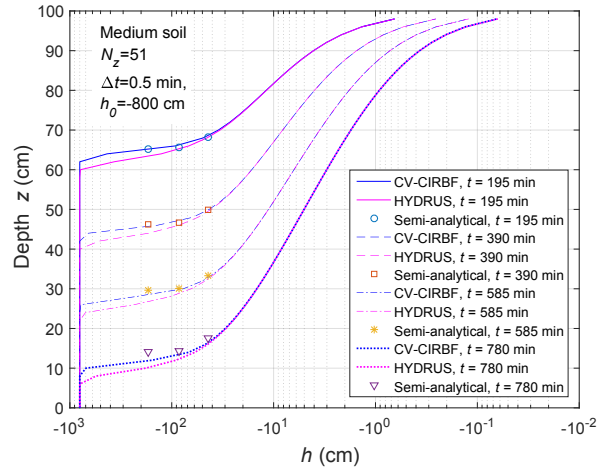
16

Figure 2. Calculated pressure head (*h*) distributions versus depth at selected times as
obtained with the CV-CIRBF scheme, the HYDRUS-1D numerical solution (Šimůnek
et al., 2008) and the semi-analytical solution of Warrick et al. (1985). Results are for
the medium-textured soil subject to ponded infiltration.

The CV-CIRBF numerical approach was also used to study infiltration in more coarse- and
fine-textured soils whose hydraulic parameters are presented in Table 1. Figures 4 and 5 show the
CV-CIRBF and HYDRUS results at different times for the coarser and finer soils, respectively,
using initial pressure heads (*h$_0$*) of -800 and -50,000 cm. Similarly as the results shown in Figs. 2
and 3, the CV-CIRBF calculations agreed well with the HYDRUS-1D results, with HYDRUS-1D
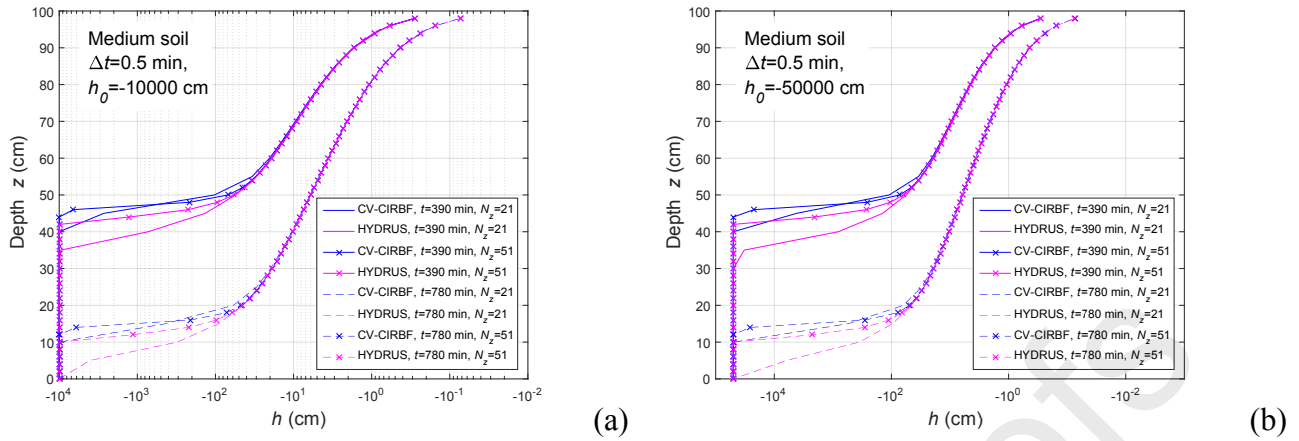again showing more of an effect of nodal spacing on the computed pressure head distributions.

17

(a)

(b)

Figure 3. Calculated pressure head (*h*) distributions versus depth at selected times for initial conditions of -10,000 cm (a) and -50,000 cm (b) as obtained with the CV-CIRBF and HYDRUS-1D numerical solutions assuming 21 and 51 nodes (grid spacings of 5 and 2 cm, respectively). Calculations are for the medium-textured soil subject to ponded infiltration.
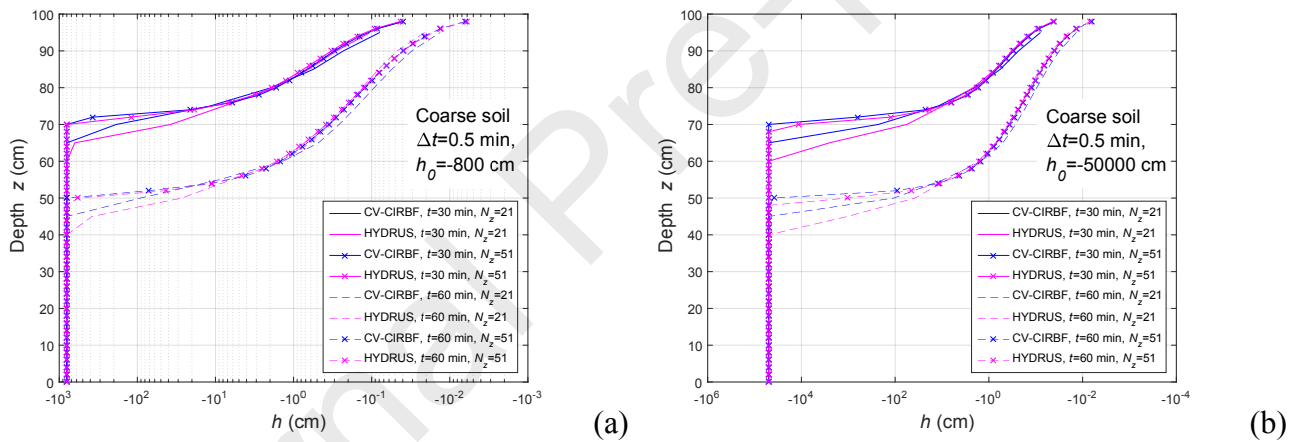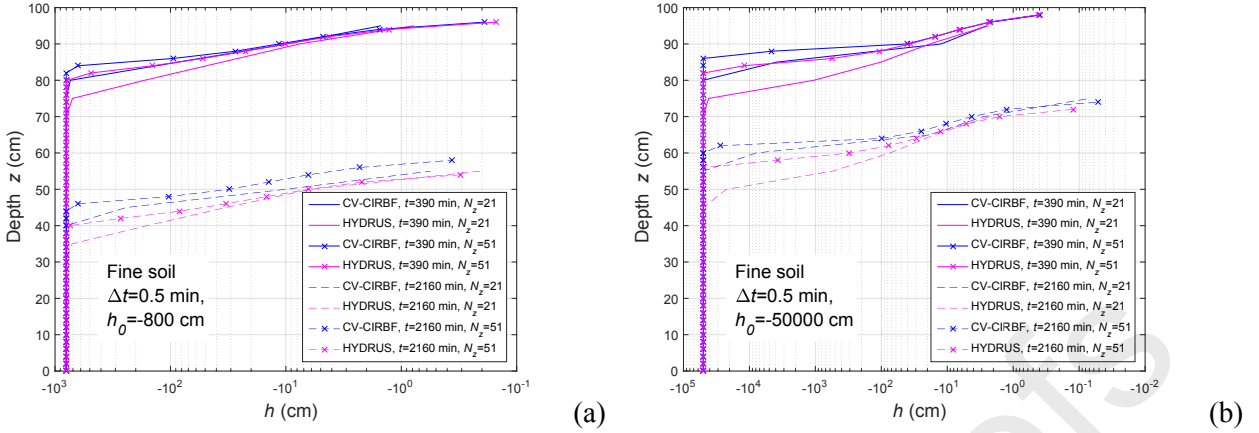

(a)

(b)

Figure 4. Calculated pressure head (*h*) distributions versus depth at selected times for initial conditions of -800 cm (a) and -50,000 cm (b) as obtained with the CV-CIRBF and HYDRUS-1D numerical solutions assuming 21 and 51 nodes (grid spacings of 5 and 2 cm, respectively). Calculations are for the coarse-textured soil subject to ponded infiltration.

Figure 5. Calculated pressure head (*h*) distributions versus depth at selected times for initial conditions of -800 cm (a) and -50,000 cm (d) as obtained with the CV-CIRBF and HYDRUS-1D numerical solutions assuming 21 and 51 nodes (grid spacings of 5 and 2 cm, respectively). Calculations are for the fine-textured soil subject to ponded infiltration.

3.2 Example 2: Constant flux at upper boundary and constant pressure head at lower boundary

In this example, we apply a constant flux at the upper boundary (q_A) and again a constant pressure head at the lower boundary (h_C). The constant flux at the upper boundary was set at half of the saturated hydraulic conductivity, i.e., $q_A = 0.5K_s$. Figure 6 shows the influence of the time step (Δt) on the CV-CIRBF results for infiltration in the medium-textured soil, in comparison also with the HYDRUS-1D solutions, assuming an initial pressure heads of -800 cm. The CV-CIRBF result became closer to the HYDRUS-1D result with reducing the time step size. We note that an adaptive time-stepping scheme was used to obtain the HYDRUS-1D result.
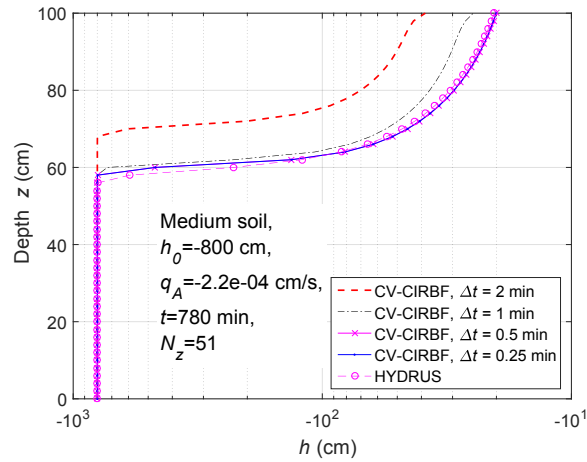
19

Figure 6. Calculated pressure head (*h*) distributions versus depth at time *t*=780 min for initial conditions of -800 cm as obtained with the CV-CIRBF and HYDRUS-1D numerical solutions assuming 51 nodes (grid spacings of 2 cm). Calculations are for the medium-textured soil subject to constant infiltration.

Figure 7 presents the CV-CIRBF and HYDRUS-1D results for infiltration into the medium-textured soil assuming initial pressure heads (h_0) of -800 and -50,000 cm, again for 21 and 51 nodes (grid spacings of 5 and 2 cm, respectively). For the calculations here we now used an adaptive time-stepping scheme to improve the computational efficiency and robustness. Following Kirkland et al. (1992), the time step (Δt) was increased by 10% when the number of Picard iterations at the previous time step was less than 4, and decreased by 10% when the number of iterations was greater than 8. The plots in Fig. 7 again show excellent agreement between the CV-CIRBF and HYDRUS-1D results, especially for the finer nodal spacing, with the CV-CIRBF distributions being less affected by the number of nodes as compared to HYDRUS-1D (especially for infiltration in the drier soil). Our CV-CIRBF solver produced a mass-conservative solution as demonstrated in Fig. 8 showing the mass balance measure (*MB*) versus time *t*. The mass balance measure is defined as $MB=m_1/m_2$ with m_1 and m_2 being the total additional mass in the domain and the total net flux into the domain, respectively. Except for some minor deviations at early times,

20

MB values were always at or very close to 1.00. Results for the coarse- and fine-textured soils were found to be very similar and are not further shown here.
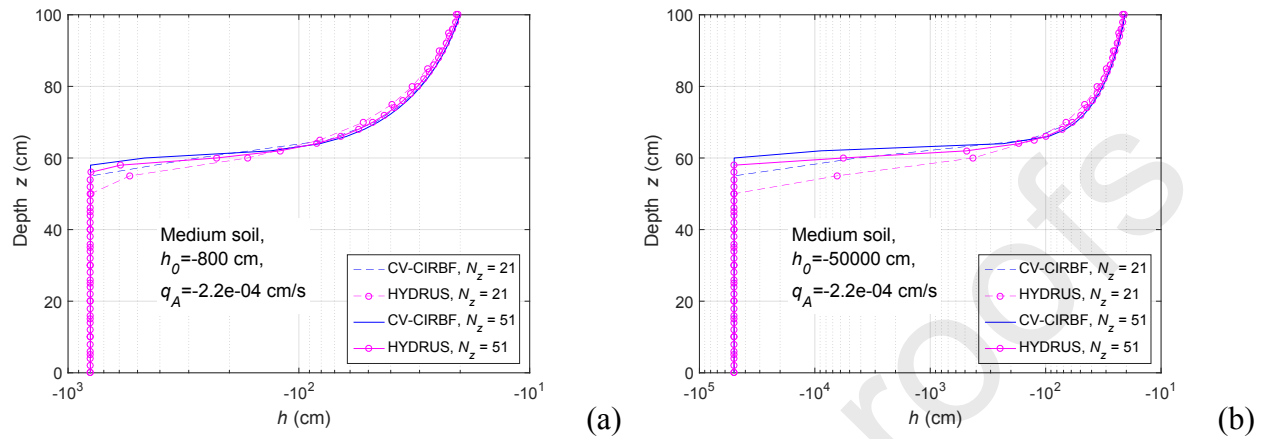

(a)   (b)

Figure 7. Calculated pressure head (*h*) distributions versus depth at time *t*=780 min for initial conditions of -800 cm (a) and -50,000 cm (d) as obtained with the CV-CIRBF and HYDRUS-1D numerical solutions assuming 21 and 51 nodes (grid spacings of 5 and 2 cm, respectively). Calculations are for the medium-textured soil subject to constant infiltration.
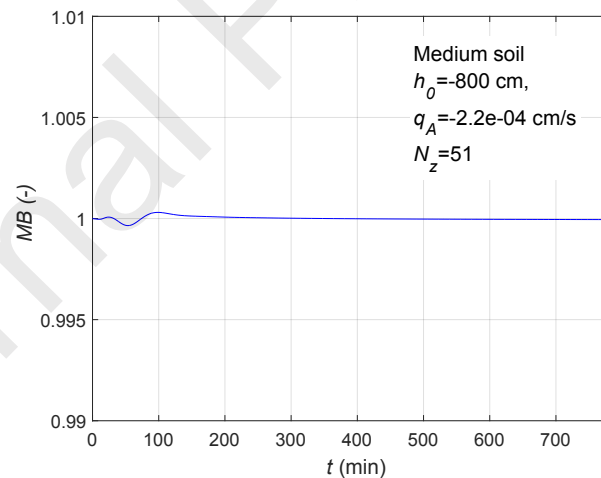

Figure 8. Calculated mass balance measure (*MB*) versus
time *t* obtained with the CV-CIRBF scheme.

21

3.3 Example 3: Flow in a layered soil with a constant flux at upper boundary and zero-flux at lower boundary

This example considers infiltration into a layered soil assuming a constant flux at the top boundary, a zero-flux at the bottom boundary, and different initial pressure heads as shown in Table 3. For the three-layered soil profile we used Berino loamy fine sand from 0 to 50 cm and 90 to 100 cm, and Glendale clay loam from 50 to 90 cm. The VG hydraulic parameters of the two soils are given in Table 4. Figure 9 presents the FDM and CV-CIRBF results for infiltration assuming an initial pressure head of -200 cm and a flux of 0.3 cm/h at the top boundary. The CV-CIRBF yielded more accurate solution than the FDM using a grid of 51 nodes. The CV-CIRBF solution using 101 nodes was almost the same as the FVM solution of McBride et al. (2006) who used a conventional finite-volume-based CFD code (Fig. 9b). Figure 10 similarly shows excellent agreement between the CV-CIRBF results and those of McBride et al. (2006) for q_A = 0.3 and 1.25 cm/h, assuming again an initial condition (h_0) of -200 cm, but also for the far more extreme case where h_0 = -50,000 cm.

Table 3. Flow in a layered soil: initial and boundary conditions, and elapsed times. Note that h_0 is the initial pressure head and q_A is the vertical flux at the top boundary.

Case	h_0 (cm)	q_A (cm/h)	Elapsed Time (h)
1	-200	0.3	4
2	-50000	0.3	12
3	-200	1.25	3.8
4	-50000	1.25	6

Table 4. Flow in a layered soil: van Genuchten soil hydraulic parameters (McBride et al., 2006).

Soil	van Genuchten hydraulic parameters				
	θ_r (cm³/cm³)	θ_s (cm³/cm³)	α (cm⁻¹)	η (-)	K_s (cm/min)
Berino loamy fine sand	0.0286	0.3658	0.0280	2.2390	0.3757
Glendale clay loam	0.1060	0.4686	0.0104	1.3954	0.0091

θ_r: residual water content; θ_s: saturated water content; α: VG multiplier of the pressure head; η: VG exponent, K_s saturated hydraulic conductivity.
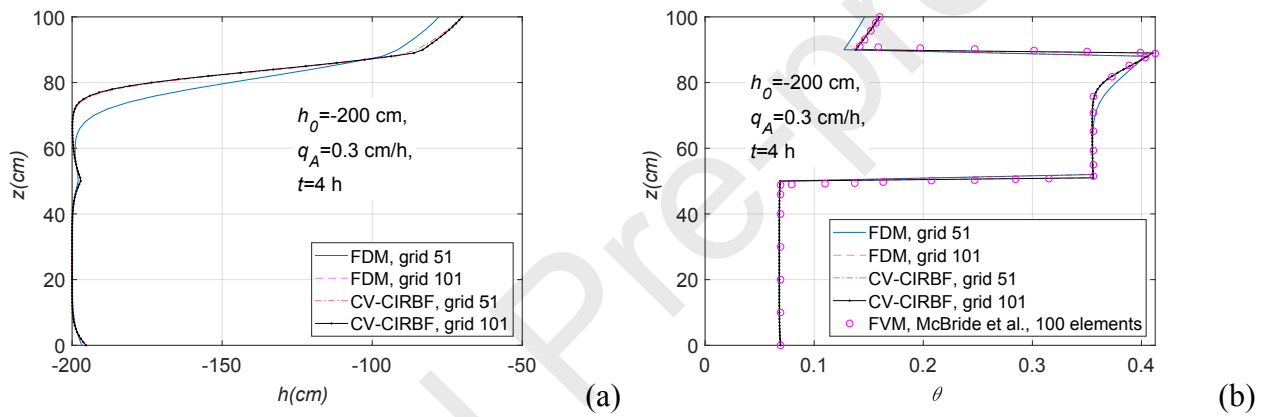

Figure 9. Calculated pressure head (a) and volumetric water content (b) distributions versus depth for Case 1 as obtained with the CV-CIRBF and FDM schemes, and the FVM solution of McBride et al. (2006) assuming 51 and 101 nodes (grid spacings of 2 and 1 cm, respectively).
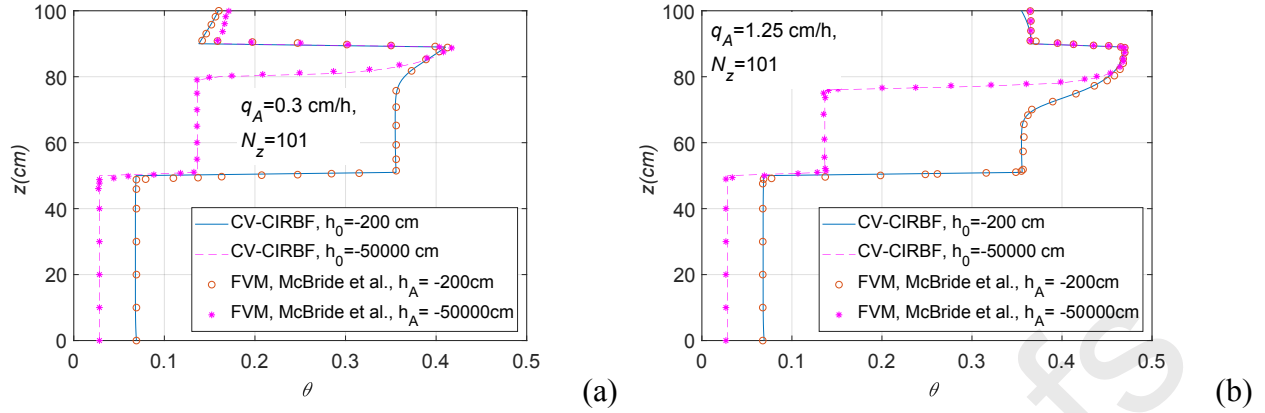
Figure 10. Calculated volumetric water content distributions versus depth for all cases as obtained with the CV-CIRBF scheme, and FVM solution of McBride et al. (2006) using 101 nodes (grid spacing of 1 cm) for the flux of 0.3 cm/h (a) and 1.25 cm/h (b) at the top boundary.

4. CONCLUSIONS

We successfully developed a control volume technique based on a compact integrated radial basis function approximation (CV-CIRBF) for solving the nonlinear Richards equation governing water flow in unsaturated and variably saturated soils. Performance of the proposed method appears satisfactory as demonstrated with ponded and constant flux infiltration in a one-dimensional vertical soil profile. The local CIRBF stencil was constructed based on information associated with three nodal points, which produced a tridiagonal system matrix similarly as with the conventional control volume method. Results showed that our calculation of internodal fluid fluxes using the global CIRBF scheme was more accurate than the approach used earlier for the local CIRBF scheme. The CV-CIRBF outperformed the FDM scheme used by Celia et al. (1990), especially when a coarser grid was used (Example 1). The proposed numerical solutions agreed well with the semi-analytical solution of Warrick et al. (1985), as well as with HYDRUS-1D results, for different boundary conditions (constant pressure heads or fluxes), initial pressure heads

24

($h_0 = -800, -10000$ and -50000 cm) and a range of soil textural classes exhibiting contrasting hydraulic behaviour. The HYDRUS-1D results closely duplicated the CV-CIRBF results only when relatively small nodal spacing were used in the HYDRUS-1D finite element solutions, with the CV-CIRBF being far less dependent upon the nodal spacing. The CV-CIRBF scheme was also used successfully to simulate flow in a layered soil profile, with its solutions being in excellent agreement with the standard FVM solutions of McBride et al. (2006). Finally, we acknowledge that in this study we limited ourselves to constant nodal spacing (Δz). Extending the solutions to irregular grid systems is relatively straightforward and has not been further addressed in this paper.

APPENDIX: COMPACT INTEGRATED RADIAL BASIS FUNCTION APPROXIMATION

The field variable u can be approximated over a compact integrated radial basis function (CIRBF) stencil corresponding to three nodal points $\{i-1, i, i+1\}$ as follows (Mai-Duy and Tran-Cong, 2013):

$$\frac{\partial^2 u(z)}{\partial z^2} = \sum_{k=i-1}^{i+1} w^{(k)} G^{(k)}(z), \tag{A.36}$$

$$\frac{\partial u(z)}{\partial z} = \sum_{k=i-1}^{i+1} w^{(k)} H_{[1]}^{(k)}(z) + c_1, \tag{A.37}$$

$$u(z) = \sum_{k=i-1}^{i+1} w^{(k)} H_{[0]}^{(k)}(z) + c_1 z + c_2, \tag{A.38}$$

where $\left\{ w^{(k)} \right\}_{k=i-1}^{i+1}$ are radial basis function (RBF) weights that need to be determined; $G^{(k)}(z)$ are known RBFs; $H_{[1]}(z) = \int G(z) dz$; $H_{[0]}(z) = \int H_{[1]}(z) dz$; and c_1 and c_2 are integration constants, which are also unknown. The RBFs $G^{(k)}(z)$ are defined as $G^{(k)}(z) = \sqrt{\left(z - z^{(k)}\right)^2 + a^{(k)2}}$ where $a^{(k)}$ is the RBF width determined presently as $a^{(k)} = \beta' g$, in which β' is a positive factor, and g the grid size. The influence of β' on the CIRBF solution accuracy was investigated in previously published papers (Hoang-Trieu et al., 2013; Mai-Duy and Tran-Cong, 2011; Mai-Duy and Tran-Cong, 2013; Ngo-Cong et al., 2017). Based on our numerical experiments, the value of β' was chosen to be 20 for the calculations in this paper. We used the nodal function values and the nodal second derivatives as extra information to construct the stencil approximations for the first and second derivatives. Application of Eq. (A.38) at three nodal points $\{i-1, i, i+1\}$ and Eq. (A.36) at two nodal points $\{i-1, i+1\}$ leads to the following system:

$$
\begin{pmatrix}
\overline{u} \\
\dfrac{\partial^2 u^{(i-1)}}{\partial z^2} \\
\dfrac{\partial^2 u^{(i+1)}}{\partial z^2}
\end{pmatrix}
=
\underbrace{
\begin{bmatrix}
H_{[0]}^{(i-1)}(z_{i-1}) & H_{[0]}^{(i)}(z_{i-1}) & H_{[0]}^{(i+1)}(z_{i-1}) & z_{i-1} & 1 \\
H_{[0]}^{(i-1)}(z_i) & H_{[0]}^{(i)}(z_i) & H_{[0]}^{(i+1)}(z_i) & z_i & 1 \\
H_{[0]}^{(i-1)}(z_{i+1}) & H_{[0]}^{(i)}(z_{i+1}) & H_{[0]}^{(i+1)}(z_{i+1}) & z_{i+1} & 1 \\
G_{[0]}^{(i-1)}(z_{i-1}) & G_{[0]}^{(i)}(z_{i-1}) & G_{[0]}^{(i+1)}(z_{i-1}) & 0 & 0 \\
G_{[0]}^{(i-1)}(z_{i+1}) & G_{[0]}^{(i)}(z_{i+1}) & G_{[0]}^{(i+1)}(z_{i+1}) & 0 & 0
\end{bmatrix}
}_{C}
\begin{pmatrix}
\overline{w} \\
\overline{c}
\end{pmatrix}
\tag{A.39}
$$

or

$$
\begin{pmatrix}
\overline{w} \\
\overline{c}
\end{pmatrix}
= C^{-1}
\begin{pmatrix}
\overline{u} & \dfrac{\partial^2 u^{(i-1)}}{\partial z^2} & \dfrac{\partial^2 u^{(i+1)}}{\partial z^2}
\end{pmatrix}^T
\tag{A.40}
$$

in which $\overline{u} = \begin{pmatrix} u^{(i-1)} & u^{(i)} & u^{(i+1)} \end{pmatrix}^T$; $\overline{w} = \begin{pmatrix} w^{(i-1)} & w^{(i)} & w^{(i+1)} \end{pmatrix}^T$ and $c = \begin{pmatrix} c_1 & c_2 \end{pmatrix}^T$. Inserting Eq. (A.40) into Eqs. (A.36) and (A.37), and applying them at nodal point i, expressions for first and second derivatives of the field variable u in physical space can be obtained:

$$
\frac{\partial^2 u^{(i)}}{\partial z^2} = \underbrace{G\left(z^{(i)}\right) C^{-1}}_{\eta}
\begin{pmatrix}
\overline{u} & \dfrac{\partial^2 u^{(i-1)}}{\partial z^2} & \dfrac{\partial^2 u^{(i+1)}}{\partial z^2}
\end{pmatrix}^T
\tag{A.41}
$$

$$
\frac{\partial u^{(i)}}{\partial z} = \underbrace{H_{[1]}\left(z^{(i)}\right) C^{-1}}_{\mu}
\begin{pmatrix}
\overline{u} & \dfrac{\partial^2 u^{(i-1)}}{\partial z^2} & \dfrac{\partial^2 u^{(i+1)}}{\partial z^2}
\end{pmatrix}^T
\tag{A.42}
$$

or

$$
\frac{\partial^2 u^{(i)}}{\partial z^2} = \eta_1 \overline{u} + \eta_2
\begin{pmatrix}
\dfrac{\partial^2 u^{(i-1)}}{\partial z^2} & \dfrac{\partial^2 u^{(i+1)}}{\partial z^2}
\end{pmatrix}^T
\tag{A.43}
$$

27

$$\frac{\partial u^{(i)}}{\partial z} = \mu_1 \overline{u} + \mu_2 \left(\frac{\partial^2 u^{(i-1)}}{\partial z^2} \quad \frac{\partial^2 u^{(i+1)}}{\partial z^2} \right)^T \tag{A.44}$$

where η and μ are known vectors of dimension of 1×5; $\eta_1 = \eta(1:3)$; $\eta_2 = \eta(4:5)$; $\mu_1 = \mu(1:3)$

and $\mu_2 = \mu(4:5)$. Equations and were solved with the Picard iteration method, with the extra

information of the second derivatives obtained from the previous iteration.

Instead of using Picard iteration, the extra information of the second derivatives in and

can be implicitly calculated using the function values at all nodes on a grid line as shown in Ngo-

Cong et al. (2017). The values of the second and first derivatives of u against z at the nodal points

on the z-grid line are then given by

$$\frac{\partial^2 \hat{u}^{(m+1)}}{\partial z^2} = \hat{D}_{2z} \hat{u}^{(m+1)}, \tag{A.45}$$

$$\frac{\partial \hat{u}^{(m+1)}}{\partial z} = \hat{D}_{1z} \hat{u}^{(m+1)}, \tag{A.46}$$

where $\hat{D}_{1z}$ and $\hat{D}_{2z}$ are fully populated $N_z \times N_z$ matrices.

REFERENCES

Carsel, R.F., Parrish, R.S., 1988. Developing joint probability distributions of soil water retention characteristics. Water Resour. Res., 24(5): 755-769. DOI:https://doi.org/10.1029/WR024i005p00755

Caviedes-Voullième, D., García-Navarro, P., Murillo, J., 2013. Verification, conservation, stability and efficiency of a finite volume method for the 1D Richards equation. J. Hydrol., 480: 69-84. DOI:10.1016/j.jhydrol.2012.12.008

Celia, M.A., Bouloutas, E.T., Zarba, R.L., 1990. A general mass-conservative numerical solution for the unsaturated flow equation. Water Resour. Res., 26(7): 1483-1496. DOI:https://doi.org/10.1029/WR026i007p01483

Divo, E., Kassab, A.J., 2007. An efficient localized radial basis function meshless method for fluid flow and conjugate heat transfer. J. Heat Transf., 129(2): 124-136. DOI:10.1115/1.2402181

Fahs, M., Younes, A., Lehmann, F., 2009. An easy and efficient combination of the mixed finite element method and the method of lines for the resolution of Richards' equation. Environ. Model. Softw., 24(9): 1122-1126. DOI:https://doi.org/10.1016/j.envsoft.2009.02.010

Farthing, M.W., Kees, C.E., Miller, C.T., 2003. Mixed finite element methods and higher order temporal approximations for variably saturated groundwater flow. Adv. Water Resour., 26(4): 373-394. DOI:https://doi.org/10.1016/S0309-1708(02)00187-2

Farthing, M.W., Ogden, F.L., 2017. Numerical solution of Richards' equation: a review of advances and challenges. Soil Sci. Soc. Am. J., 81(6): 1257-1269. DOI:10.2136/sssaj2017.02.0058

Hayek, M., 2016. An exact explicit solution for one-dimensional, transient, nonlinear Richards' equation for modeling infiltration with special hydraulic functions. J. Hydrol., 535: 662-670. DOI:https://doi.org/10.1016/j.jhydrol.2016.02.021

Hoang-Trieu, T.-T., Mai-Duy, N., Tran, C.-D., Tran-Cong, T., 2013. A finite-volume method based on compact local integrated radial basis function approximations for second-order differential problems. CMES: Comput. Model. Eng. Sci., 91(6): 485-516. DOI:10.3970/cmes.2013.091.485

Hon, Y.-C., Šarler, B., Yun, D.-f., 2015. Local radial basis function collocation method for solving thermo-driven fluid-flow problems with free surface. Eng. Anal. Bound. Elem., 57: 2-8. DOI:https://doi.org/10.1016/j.enganabound.2014.11.006

Huang, K., Mohanty, B., Van Genuchten, M.T., 1996. A new convergence criterion for the modified Picard iteration method to solve the variably saturated flow equation. J. Hydrol., 178(1-4): 69-91. DOI:https://doi.org/10.1016/0022-1694(95)02799-8

Kansa, E.J., 1990. Multiquadrics - A scattered data approximation scheme with applications to computational fulid-dynamics - II: Solutions to parabolic, hyperbolic and elliptic partial differential equations. Comput. Math. Appl., 19 (8-9): 147-161. DOI:https://doi.org/10.1016/0898-1221(90)90271-K

Kavetski, D., Binning, P., Sloan, S., 2001. Adaptive time stepping and error control in a mass conservative numerical solution of the mixed form of Richards equation. Adv. Water Resour., 24(6): 595-605. DOI:https://doi.org/10.1016/S0309-1708(00)00076-2

Kirkland, M.R., Hills, R., Wierenga, P., 1992. Algorithms for solving Richards' equation for variably saturated soils. Water Resour. Res., 28(8): 2049-2058. DOI:https://doi.org/10.1029/92WR00802

Lehmann, F., Ackerer, P., 1998. Comparison of iterative methods for improved solutions of the fluid flow equation in partially saturated porous media. Transp. Porous Media, 31(3): 275-292. DOI:https://doi.org/10.1023/A:1006555107450

Mai-Duy, N., Tran-Cong, T., 2001. Numerical solution of Navier-Stokes equations using multiquadric radial basis function networks. Int. J. Numer. Methods Fluids, 37(1): 65-86. DOI:https://doi.org/10.1002/fld.165

Mai-Duy, N., Tran-Cong, T., 2011. Compact local integrated-RBF approximations for second-order elliptic differential problems. J. Comput. Phys., 230(12): 4772-4794. DOI:https://doi.org/10.1016/j.jcp.2011.03.002

Mai-Duy, N., Tran-Cong, T., 2013. A compact five-point stencil based on integrated RBFs for 2D second-order differential problems. J. Comput. Phys., 235: 302-321. DOI:https://doi.org/10.1016/j.jcp.2012.10.048

McBride, D., Cross, M., Croft, N., Bennett, C., Gebhardt, J., 2006. Computational modelling of variably saturated flow in porous media with complex three-dimensional geometries. Int. J. Numer. Methods Fluids, 50(9): 1085-1117. DOI:https://doi.org/10.1002/fld.1087

Ngo-Cong, D. et al., 2017. A generalised finite difference scheme based on compact integrated radial basis function for flow in heterogeneous soils. Int. J. Numer. Methods Fluids, 85(7): 404-429. DOI:https://doi.org/10.1002/fld.4386

Pan, L., Wierenga, P.J., 1995. A transformed pressure head-based approach to solve Richards' equation for variably saturated soils. Water Resour. Res., 31 (4): 925-931. DOI:https://doi.org/10.1029/94WR03291

Phoon, K.-K., Tan, T.-S., Chong, P.-C., 2007. Numerical simulation of Richards equation in partially saturated porous media: under-relaxation and mass balance. Geotech. Geol. Eng., 25(5): 525-541. DOI:https://doi.org/10.1007/s10706-007-9126-7

Šarler, B., Vertnik, R., 2006. Meshfree explicit local radial basis function collocation method for diffusion problems. Comput. Math. Appl., 51(8): 1269-1282. DOI:https://doi.org/10.1016/j.camwa.2006.04.013

Schaap, M.G., Leij, F.J., Van Genuchten, M.T., 2001. Rosetta: A computer program for estimating soil hydraulic parameters with hierarchical pedotransfer functions. J. Hydrol., 251(3-4): 163-176. DOI:https://doi.org/10.1016/S0022-1694(01)00466-8

Šimůnek, J., Šejna, M., Saito, H., Sakai, M., Van Genuchten, M.T., 2008. The HYDRUS-1D software package for simulating the movement of water, heat, and multiple solutes in variably saturated media, version 4.0: HYDRUS Software Series 3. Department of Environmental Sciences, University of California Riverside, Riverside, California, USA, 315.

van Genuchten, M.T., 1980. A closed-form equation for predicting the hydraulic conductivity of unsaturated soils. Soil Sci. Soc. Am. J., 44(5): 892-898. DOI:10.2136/sssaj1980.03615995004400050002x

van Genuchten, M.T., 1982. A comparison of numerical solutions of the one-dimensional unsaturated—saturated flow and mass transport equations. Adv. Water Resour., 5(1): 47-55. DOI:https://doi.org/10.1016/0309-1708(82)90028-8

Vertnik, R., Mramor, K., Šarler, B., 2019. Solution of three-dimensional temperature and turbulent velocity field in continuously cast steel billets with electromagnetic stirring by a meshless method. Eng. Anal. Bound. Elem., 104: 347-363. DOI:https://doi.org/10.1016/j.enganabound.2019.03.026

Vogel, T., Hopmans, J.W., 1992. Two-dimensional analysis of furrow infiltration. J. Irrig. Drain Eng., 118 (5): 791-806. DOI:https://doi.org/10.1061/(ASCE)0733-9437(1992)118:5(791)

Warrick, A., Lomen, D., Yates, S., 1985. A generalized solution to infiltration. Soil Sci. Soc. Am. J., 49(1): 34-38. DOI:10.2136/sssaj1985.03615995004900010006x

Wright, G.B., Fornberg, B., 2006. Scattered node compact finite difference-type formulas generated from radial basis functions. J. Comput. Phys., 212(1): 99-123. DOI:https://doi.org/10.1016/j.jcp.2005.05.030

Younes, A., Ackerer, P., Lehmann, F., 2006. A new mass lumping scheme for the mixed hybrid finite element method. Int. J. Numer. Methods Eng., 67(1): 89-107. DOI:https://doi.org/10.1002/nme.1628

Zha, Y. et al., 2019. Review of numerical solution of Richardson–Richards equation for variably saturated flow in soils. Wiley Interdiscip. Rev.: Water: e1364. DOI:https://doi.org/10.1002/wat2.1364

Declaration of interests

☒ The authors declare that they have no known competing financial interests or personal relationships that could have appeared to influence the work reported in this paper.

☐The authors declare the following financial interests/personal relationships which may be considered as potential competing interests:

Declaration of interests

☒ The authors declare that they have no known competing financial interests or personal relationships that could have appeared to influence the work reported in this paper.

☐The authors declare the following financial interests/personal relationships which may be considered as potential competing interests:

Highlights

- A new control volume scheme was developed to solve the nonlinear Richards equation.
- The scheme was constructed using compact integrated radial basis function stencils.
- Different initial and boundary conditions and soil textural classes were investigated.
- Results were in good agreement with Warrick's semi-analytical solutions.
- Results were less dependent on the grid spacing than those of HYDRUS-1D.